Direct BEM for high-resolution global gravity field modelling

R. Čunderlík, K. Mikula

Dept. of Mathematics and Descriptive Geometry, Faculty of Civil Engineering, Slovak University of Technology, Radlinského 11, 813 68 Bratislava, Slovakia
e-mail: cunderli@svf.stuba.sk, mikula@math.sk

Abstract. The paper presents a high-resolution global gravity field modelling by the boundary element method (BEM). A direct BEM formulation for the Laplace equation is applied to get a numerical solution of the linearized fixed gravimetric boundary-value problem. The numerical scheme uses the collocation method with linear basis functions. It involves a discretization of the complicated Earth's surface, which is considered as a fixed boundary. Here 3D positions of collocation points are simulated from the DNSC08 mean sea surface at oceans and from the SRTM30PLUS_V5.0 global topography model added to EGM96 on lands. High-performance computations together with an elimination of the far zones' interactions allow a very refined integration over the all Earth's surface with a resolution up to 0.1 deg. Inaccuracy of the approximate coarse solutions used for the elimination of the far zones' interactions leads to a long-wavelength error surface included in the obtained numerical solution. This paper introduces an iterative procedure how to reduce such long-wavelength error surface. Surface gravity disturbances as oblique derivative boundary conditions are generated from the EGM2008 geopotential model. Numerical experiments demonstrate how the iterative procedure tends to the final numerical solutions that are converging to EGM2008. Finally the input surface gravity disturbances at oceans are replaced by real data obtained from the DNSC08 altimetry-derived gravity data. The ITG-GRACE03S satellite geopotential model up to degree 180 is used to eliminate far zones' interactions. The final high-resolution global gravity field model with the resolution 0.1 deg is compared with EGM2008.

Keywords: Global Gravity Field Modelling – Fixed Gravimetric Boundary Value Problem – Boundary Element Method – Elimination of Far Zones' Interactions – Iterative Reducing of Long-Wavelength Error Surface

1 Introduction

Precise global gravity field modelling is mainly performed by spherical harmonics (SH). Satellite missions that permanently monitor a long-wavelength part of the gravity field yield the satellite geopotential models. Here the coefficients of lower degree and order are very precisely obtained, however overall accuracy of such satellite models is usually not sufficient for some investigations in geodesy, e.g. for the vertical datum problem and a unification of vertical systems. For such purposes a short-wavelength part of the gravity field (considered in a global sense) needs to be determined as precise as possible. For SH-based methods, that use basis functions with the global support, it means a sophisticated evaluation of the higher degree coefficients. Here recently released EGM2008 up to degree 2160 (Pavlis et al. 2008) represents a significant improvement in resolution and precision of the geopotential models.

Nowadays, an efficiency of numerical methods like the boundary element method (BEM), finite element method (FEM) or finite volume method (FVM) has rapidly increase with a development of HPC (high-performance computing) facilities. Opportunities for large-scale and parallel computations make these methods applicable also for the precise global

gravity field modelling. In contrary to the methods that use global basis functions like SH, the aforementioned numerical methods allow to use basis functions with local supports like finite elements. It has an advantage, that a successive refinement of the discretization is very straightforward and in general improves precision of numerical results. The price to be paid is large memory requirements. This drawback can be overcome by parallel computing and compression techniques like the fast multipole method (FMM) (Greengard and Rokhlin 1987), panel clustering (Hackbusch and Nowak 1989), wavelet techniques (e.g. (Mallat, 1989), (Barthelmes et al. 2004)) and others, e.g. an iterative treatment for the elimination of far zones' interactions introduced in this paper.

The first applications of FEM to the gravity field modelling was given by Meissl (1981) and Shaofeng and Dingbo (1991). Recently, FEM and FVM applied in physical geodesy have been discussed in (Fašková et al. 2007) and (Fašková 2008). In case of BEM, the first application was given by Klees (1992). This approach based on the indirect BEM formulation and the Galerkin BEM was gradually extended (Lehmann and Klees 1996), (Lehmann 1997), (Klees, 1998) until the sophisticated level (Klees et al. 2001) where the panel clustering and FMM were implemented to reduce a numerical complexity of BEM. Later on, the direct BEM formulation for the fixed gravimetric boundary-value problem (FGBVP) based on the collocation with linear basis functions was published in (Čunderlík et al. 2008). Here an elimination of far zones' interactions using approximate coarse solutions was introduced to reduce large memory requirements. In this paper we complete such simple elimination approach by an iterative procedure that is necessary to reduce a long-wavelength error surface that arises from inaccuracy of approximate values obtained from numerical solutions on coarser grids or from the satellite geopotential models. Results of the numerical experiments show how the iterative procedure reduces this error.

A goal of this paper is also to present a high-resolution numerical solution to the linearized FGBVP using the direct BEM formulation and new sources of gravity data, namely the DNSC08 gravity field model (Andersen at al. 2008), the EGM2008 geopotential model (Pavlis et al. 2008) and the ITG-GRACE03S satellite geopotential model (Mayer-Gürr 2007). An access to HPC facilities, parallel computing and the elimination of far zones' interactions allow us to reduce enormous memory requirements and thus increase a level of discretization up to 0.1 deg, which is comparable with a resolution of EGM2008. Since the DNSC08 altimetry-derived gravity data represents real input data at oceans, the high-resolution numerical solution obtained by BEM is compared with EGM2008, the most detailed global gravity field model at present.

Our motivation to work in the framework of the fixed gravimetric BVP results from the fact that surface gravity disturbances are globally consistent and fully independent from levelling. So far, such approach represents an idealization since a majority of terrestrial gravimetric measurements collected for decades have been accompanied by levelling. However, shifts and tilts of local vertical datums make gravity anomalies globally inconsistent that can mislead the precise global solutions based on integration over the Earth's surface. In contrary, the precise 3D positioning by GNSS has brought a striking advantage that all terrestrial gravity data can have the consistent vertical information. Such benefit is promising for precise gravity field modelling in future and motivates to solve the fixed gravimetric BVP.

2 The direct BEM for the linearized fixed gravimetric BVP

Let us briefly outline the direct BEM formulation for FGBVP. The linearized FGBVP represents an exterior oblique derivative problem for the Laplace equation, cf. (Koch and Pope 1972), (Bjernhammar and Svensson 1983) or (Grafarend 1989)

$$\Delta T(\boldsymbol{x}) = 0, \qquad \boldsymbol{x} \in R^3 - \Omega, \tag{1}$$

$$\langle \nabla T(\boldsymbol{x}), s(\boldsymbol{x}) \rangle = -\delta g(\boldsymbol{x}), \quad \boldsymbol{x} \in \Gamma, \tag{2}$$

$$T = O(|x|^{-1}) \quad as \quad x \to \infty \tag{3}$$

where T is the disturbing potential at any point $\boldsymbol{x}$, δg is the surface gravity disturbance, the domain Ω represents the body of the Earth with its boundary Γ (the Earth's surface), $\langle\ ,\ \rangle$ is the inner product of two vectors and

$$\boldsymbol{s(x)} = -\nabla U(\boldsymbol{x}) / |\nabla U(\boldsymbol{x})|, \qquad \boldsymbol{x} \in \Gamma, \tag{4}$$

where U is the normal gravity potential. Eq. (2) represents the oblique derivative boundary condition (BC) as the normal to the Earth's surface Γ does not coincide with the vector $\boldsymbol{s}$ defined by Eq. (4).

The direct BEM formulation for the Laplace equation leads to a boundary integral equation (BIE) that can be derived using Green's third identity or through the method of weighted residual, cf. e.g. (Brebbia et al. 1984) or (Schatz et al. 1990). A main advantage arises from the fact that only the boundary of the solution domain requires a subdivision into its elements. Thus the dimension of the problem is effectively reduced by one. The direct BEM formulation applied to the linearized FGBVP in Eq. (1-3) results in BIE in the form

$$\frac{1}{2} T(\boldsymbol{x}) + \int_{\Gamma} T(\boldsymbol{y}) \frac{\partial G}{\partial n_\Gamma}(\boldsymbol{x}, \boldsymbol{y})\, d\boldsymbol{y} = \int_{\Gamma} \frac{\partial T}{\partial n_\Gamma}(\boldsymbol{y})\, G(\boldsymbol{x}, \boldsymbol{y})\, d\boldsymbol{y}, \qquad \boldsymbol{x} \in \Gamma, \tag{5}$$

where $\boldsymbol{n_\Gamma}$ is the normal to the boundary Γ (the Earth's surface) and the kernel function G represents the fundamental solution of the Laplace equation,

$$G(\boldsymbol{x}, \boldsymbol{y}) = (4\pi\, |\boldsymbol{x} - \boldsymbol{y}|\,)^{-1}, \qquad \boldsymbol{x}, \boldsymbol{y} \in R^3. \tag{6}$$

In order to handle the oblique derivative problem we use the same simplification as we proposed in (Čunderlík et al. 2008). According to the oblique derivative BC in Eq. (2), $\nabla T(\boldsymbol{x})$ projected to $\boldsymbol{s(x)}$ equals to $-\delta g(\boldsymbol{x})$. Then the normal derivative term $\partial T/\partial n_\Gamma$ in BIE (5) is approximately equal to $-\delta g(\boldsymbol{x})\cos\mu(\boldsymbol{x})$, where $\mu(\boldsymbol{x})$ is the angle $\angle(\boldsymbol{n_\Gamma(x)}, \boldsymbol{s(x)})$. Let us note that this term represents the projection of the vector $\delta g(\boldsymbol{x})\boldsymbol{s(x)}$ (not exactly of the vector $\nabla T(\boldsymbol{x})$) to the normal $\boldsymbol{n_\Gamma(x)}$. In this way the oblique derivative BC in Eq. (2) is incorporated into the direct BEM formulation in BIE (5). Such approach includes an error from neglecting the tangential components of the oblique derivative. Another approach based on a decomposition of the oblique derivative into the normal and tangential components is described in e.g. (Baláš et al. 1989).

As a numerical technique we use the collocation method with linear basis functions. (Remark: in our approach we use the collocation despite the fact that there is only numerical evidence and no mathematical prove of convergence of the collocation for the oblique-type integral equation of the second type.) Such collocation involves a discretization of the complicated Earth's surface by a triangulation of the topography and approximations of the boundary functions by a linear function on each triangular panel using linear basis functions. It means the piecewise linear polynomials defined on the planar triangular panels are being used, where vertices of this triangulation represent the collocation points. In such a way we get a discrete form of BIE (5) that subsequently yields a linear system of equations,

$$M \, t \ = \ L \, \delta g \, , \tag{7}$$

where t is the vector of unknown disturbing potential at the collocation points and δg is the vector of the input surface gravity disturbances. The coefficients of matrices M and L represent integrals of the discrete form of BIE (5) that need to be computed using an appropriate discretization of the integral operators, for more details see (Čunderlík et al. 2008). Since the kernel functions in BIE (5) depend on direct distances only, components of both matrices M and L are given only by the geometry of the fixed Earth's surface, i.e. they are invariant with respect to the input BC. In our case we consider the oblique derivative BC in Eq.(2), or rather the Neumann BC using the aforementioned projection. Then matrix M represents a system matrix, while the known vector $f = L \delta g$ is given on the right-hand side of Eq.(7).

3 Experimental order of convergence

In order to illustrate the order of convergence of the numerical scheme, we perform the following experiment. Let us suppose the gravitational potential generated by an artificial sphere. Let this sphere have parameters adopted from the real Earth, i.e. the geocentric gravitational constant $GM = 398\ 600.5$ $km^3.s^{-2}$ and the radius R = 6 371 km. Hence, the gravitational potential on the sphere surface equals to $GM/R = 62.564\ 824\ 988$ $km^2.s^{-2}$ (the exact solution) and the Neumann BC equals to $-GM/R^2 = -9.82$ $m.s^{-2}$. Then we perform numerical experiments by BEM for different levels of the discretization of the sphere.

Now let us assume that the error of the scheme in some norm is proportional to some power of the mesh size h, i.e., $Error(h) = Ch^{\alpha}$, with a constant C. Halving the mesh size we get $Error(h/2) = C(h/2)^{\alpha}$, from where we can simply extract $\alpha = log_2(Error(h)/\ Error(h/2))$. The α is called the experimental order of convergence (EOC) and can be determined by comparing numerical solutions with the exact solutions. Table 1 shows a bias of the obtained numerical solutions, the L2-norm of residuals from the exact solution and EOC. It is evident that the numerical shceme by the direct BEM is second order accurate (Tab.1).

4 Elimination of far zones' interactions

The system matrix M is dense and nonsymmetric, therefore a successive refinement of the discretization leads to large memory requirements. This drawback can be efficiently overcome by parallel computing and by compression techniques like the fast multipole method (FMM) (Greengard and Rokhlin 1987), panel clustering (Hackbusch and Nowak 1989), wavelet-based compression techniques (e.g. (Mallat, 1989), (Barthelmes et al. 2004)) and others. In (Čunderlík et al. 2008) we proposed a simple elimination of far zones' interaction using approximate values of the unknown disturbing potential from numerical solutions on coarser grids or from the known geopotential models. It means, considering properties of the kernel function $\partial G/\partial n_\Gamma$ in BIE (5), all the matrix components corresponding to far zones' interactions can be multiplied by the approximated values and passed to the vector f on the right-hand side. In this way the dense system matrix is truncated into the sparse one. Such approach can rapidly reduce large memory requirements, although the CPU time consumption remains almost unchanged. In such approach inaccuracy of the approximate values can yield a long-wavelength error surface (LWES) included in the obtained numerical solution. This LWES can be reduced using an iterative procedure

$$M_{NZ} \, t^i \ = \ f \, - \, M_{FZ} \, t^{i-1} \, , \tag{8}$$

where M_{FZ} is the matrix of far zones' interactions, $M_{NZ} = (M - M_{FZ})$ is the new sparse system matrix including only components of near zones' interactions, the vector t^i represents the unknown disturbing potential in the i-th iteration and t^{i-1} includes the approximate values

obtained from the previous iterative step. In the first iterative step the approximate values can be obtained from numerical solutions by BEM on coarser grids or from the known geopotential models. In this paper we deal with numerical experiments showing how LWES of the obtained numerical solutions is reduced by the iterative procedure (8) tending to certain values. We experimentally test such tending for different levels of the discretization, different distance criteria for far zones and different sources of the approximate values used for far zones' interactions in the first iterative step.

5 High resolution gravity field modelling

Next numerical experiments deal with the global gravity field modeling. The Earth's surface as a fixed boundary is approximated by a triangulated surface. Vertices of this triangulation represent collocation points. Their horizontal positions are generated by the developed algorithm (Čunderlík et al. 2002). Vertical positions are interpolated from the following datasets. At oceans/seas we use the DNSC08 mean sea surface (Andersen et al. 2008). On lands we add the SRTM30_PLUS V5.0 global topography model (Becker at al. 2009) to the EGM-96 geoid heights (Lemoine et al. 1998). In this way we get geocentric positions of the collocation points, i.e. the precise 3D position of the approximated Earth's surface.

In our numerical experiments we use different levels of the discretization according to the available internal memory of our cluster (128 GB for long jobs, exceptionally 256 GB for short jobs). Table 2 depicts the used discretization levels and corresponding memory requirements in case of the dense system matrix or for the sparse one specifying the distance criterion for far zones. This criterion is chosen in order not to overstep the available memory limit 128 GB taking into account memory requirements necessary for auxiliary variables (Tab.2, the last three columns).

All numerical experiments can be divided into two groups. In the first group we experimentally test the iterative procedure (8) for three aforementioned factors (Chapter 4). Here the surface gravity disturbances as the input boundary conditions in the collocation points are generated from EGM2008. Consequently, the numerical solutions by BEM are assumed to converge to EGM2008. In the second group of the numerical experiments we replace the surface gravity disturbances at oceans/seas by values evaluated from the DNSC08 gravity anomaly dataset. Such gravity data can be considered as real input data at oceans. Then we are interesting how the obtained BEM solution differs from EGM2008, the most detailed and precise global gravity field model at present.

After preparing input data we perform several large-scale parallel computations for different discretization levels (Tab.2) using the standard MPI (Message Passing Interface) subroutines (Aoyama and Nakano 1999). All obtained numerical solutions are compared with EGM2008. Statistical characteristics of residuals are considered as quality criteria. In the first group of experiments, where the setup is generated from EGM2008, we test how LWES is reduced by the iterative procedure (8). For such purposes we consider the residuals only at oceans due to the fact that our numerical solutions are computed at points on the complicated Earth's surface, and high residuals in extremely mountainous regions could significantly influence our estimations.

In case of the resolution 0.2 deg (Tab.2, 1 215 002 collocation points) we test an iterative procedure for different sources of approximate values used in the first iterative step. We consider two cases of such approximate values, i.e., (i) obtained from the finest numerical solution by BEM with the dense system matrix (the resolution 0.523 deg and 177 506 collocation points (Tab.4)), and (ii) obtained from the ITG-GRACE03S satellite geopotential model (Mayer-Gürr 2007) up to degree 180. It is evident (Fig.1) that in both cases method

tends to the same value. More precise approximate values from ITG-GRACE03S lead to the smaller LWES in the first iterative step, which is more appropriate to reach the final solution.

Figure 2 shows how a speed of tending is changing using different distance criteria for far zones. In case of the resolution 0.36 deg we compare results of the iterative procedure (8) for three different distance criteria: 3 189 km ($a/2$), 1 595 km ($a/4$) and 911 km ($a/7$), where a is the semimajor axis of the reference ellipsoid. Apparently, the speed of tending is higher for the bigger distance criterion (Fig.2). In case of the biggest distance criterion the standard deviations are almost the same in each iterative step, while for the smaller distance criteria they are slightly improved from worse values in the first iterative steps (Fig.2).

All these experiences encouraged us to refine the discretization of the Earth's surface up to the resolution 0.1 deg (Tab.2, 4 860 002 collocation points), which is comparable with the resolution of EGM2008 (SH up to degree and order 2160). In comparison with the resolution 0.2 deg, such refinement implies an increase of the collocation points by the factor 4 and an increase of memory requirements as well as CPU time by the factor 16 (Tab.2). Consequently the distance criterion for far zones needs to be decreased from 911 km ($a/7$) to 213 km ($a/30$) due to the available memory limit 128 GB (Tab.2). Approximate values obtained from ITG-GRACE03S are used for the elimination of far zone's interactions in the first iterative step. A slow speed of tending due to the small distance criterion for far zones forced us to use an average of the 3rd and 4th iterations as approximate values for the next iterative step (Fig.3, Tab.3). Since the additional iterations do not change the results considerably, we stop the process in the 6th iterative step. The residuals between the obtained numerical solution by BEM and EGM2008 are depicted in Fig.4a. Figure 5 shows LWES as a difference between the numerical solutions in the last and first iterative steps.

In order to illustrate how a precision of numerical results increases by refining the distretization of the Earth's surface, we summarize statistical characteristics of residuals between the numerical solutions by BEM and EGM2008 for different levels of the discretization (Tab.4). The first two columns represent large-scale computations with the dense system matrix and the last three columns correspond to more refined discretization levels using the elimination of far zones' interactions and the iterative procedure (8). It is evident that a successive refinement of the discretization results in decreasing of all statistical characteristics, i.e., step by steps leads to more precise numerical solutions. The final mean values of residuals (after reducing LWES by the iterative procedure) indicate that numerical solutions on coarser grids include an overall shift. This shift is decreasing by refining the discretization. Table 4 also shows computational aspects like a number of processors used for parallel computations, necessary memory requirements, CPU time for the matrix assembling and the BiCGSTAB linear solver as well as the total CPU time per processor.

Finally we perform the same numerical experiment with the resolution 0.1 deg replacing the surface gravity disturbances at oceans by values evaluated from DNSC08. According to authors (Andersen et al. 2008), DNSC08_GRAV includes the altimetry-derived free-air gravity anomalies at oceans/seas augmented by EGM2008 on lands. Thus for our purposes we interpolate the free-air gravity anomalies Δg in the collocation points from DNSC08_GRAV and transform them into the surface gravity disturbances using EGM2008,

$$\delta g(\boldsymbol{x}) \ = \ \Delta g^{DNSC08}(\boldsymbol{x}) \ + \ 0.30855 \ \zeta^{EGM2008}(\boldsymbol{x}) \ , \quad [mGal] \qquad (9)$$

where $\zeta^{EGM2008}$ is the height anomaly evaluated from EGM2008 up to degree 2160. Differences between the free-air gravity anomalies and surface gravity anomalies, relevant only on lands, are neglected.

Statistical characteristics of residuals at collocation points between numerical solutions in each iterative step and EGM2008 are depicted in Fig.3 and Tab.3. The residuals between the final numerical solution and EGM2008 are depicted in Fig.4b. A detail view of maximal and minimal residuals in Himalayas is shown in Fig.6. Figure 7 depicts the profiles of both solutions, numerical solution by BEM and EGM2008, as well as their residuals in this extremely mountainous region. Afterwards, the geopotential on the DNSC08 mean sea surface is computed from the obtained disturbing potential. Since the DNSC08 altimetry-derived gravity data represents a real input data at oceans, we present how the computed geopotential agree with one evaluated from EGM2008. Figure 8 shows its overall behavior for both gravity field models. Details at different oceans are depicted in Fig.9.

6 Discussions

Presented numerical experiments demonstrate a possibility of the proposed approach for the high-resolution global gravity field modelling. The elimination of far zones' interactions using approximate values from satellite geopotential models and the iterative treatment can efficiently reduce enormous memory requirements and thus overcome a main drawback of BEM applications. In a comparison with FMM (Greengard and Rokhlin 1987), our approach is not so efficient in terms of CPU time consumption but it can reduce memory requirements slightly better, since it does not require extra memory for auxiliary variables necessary to perform FMM in 3D (octrees clustering, spherical harmonics and expansions coefficients). On the other hand, our approach lacks an estimate of the approximation error that exists for FMM, the panel clustering or wavelet-based compression technique. The converging behavior of the iterative procedure is here demonstrated by the presented numerical experiments.

Hence, the iterative procedure is mainly influenced by three aforementioned factors. The higher distance criterion for far zones makes the linear system in Eq. (8) closer to the original one in Eq. (7). Therefore a speed of tending is faster and only few iterations are necessary to obtain a final result (Fig.2). On the other side, this distance criterion needs to be set for a particular discretization level in order not to overstep a memory limit of available computer facilities. Consequently, we are forced to take a small distance criterion for a very refined discretization, which makes a tending speed slower. In this case it is possible to speed up a process by averaging results from last two iterative steps and use it for next iteration (Fig.3, Tab.3).

Accuracy of the approximate values used in the first iterative step has an essential impact on an initial LWES of the numerical solution that is later reduced by the iterative procedure (8). Therefore a final numerical solution can be obtained faster when using more precise approximate values in the first iteration. According to our experience, recent satellite geopotential models, e.g. ITG-GRACE03S up to degree 180, offer more precise approximate values used in the first iteration than our numerical solutions by BEM with the dense system matrix computed on coarse grids (Fig.1).

A level of the discretization is fundamental for a precision of the obtained numerical results (Tab.4). A more refined discretization leads to a more precise solution despite the fact that the distance criterion has to be decreased (compare values in Fig.1-3). This is promising for further increasing of the resolution. Here we would like to emphasize that successive refining of the discretization is very straightforward and step by step makes the problem closer to reality. The only limit is memory availability, which is more technical problem. In this context, recent developments of HPC facilities are bringing new opportunities.

The final gravity field models represent the numerical solutions to FGBVP by the direct BEM with the resolution 0.1 deg. Their comparison with EGM2008 at the collocation

points shows that agreement is better at oceans (Fig.4, Tab.3). For the test setup generated from EGM2008 the standard deviation of residuals at oceans is 0.055 GPU (1 GPU = 10 $m^2.s^{-2}$). In case that the DNSC08 altimetry-derived gravity data are used at oceans, the standard deviation is 0.077 GPU. Here negative residuals in area of the global minimum (south of India) and positive residuals in area of the global maximum (Oceania) ranging up to ±0.3 GPU indicates a small discrepancy (Fig.4b). This discrepancy can also be notices as a slightly different behavior of the geopotential on the DNSC08 mean sea surface (Fig.8-9). Taking into account that long-wavelength part of gravity field is very precisely obtained from satellite missions, this discrepancy is probably caused by the inaccurate transformation (Eq. (9)) of the altimetry-derived free-air gravity anomalies into the surface gravity disturbances using different parameters of the reference field.

For both setups, statistical characteristics of residuals on lands are worse. The standard deviation about 0.14 GPU (Tab.4, the last column) is negatively affected by the high residuals in extremely mountainous areas, especially in Himalayas and Andes (Fig.4). Here we remind that the numerical solution is computed at points on the complicated Earth's surface. A detail view of the residuals in Himalayas (Fig.6) and the profiles across both solutions (Fig.7) show high positive residuals up to 3.7 GPU correlating with the topography of the main range of Himalayas and negative residuals up to -1.4 GPU in the negative isostatic zones around the Tibetan plateau. Surprisingly, analyzing the profile across the main range of Himalayas (Fig.7, at the bottom), local minimums are almost identical, while local maximums are significantly higher in case of the numerical solution by BEM.

Comparing the achieved numerical results with previous ones published in (Čunderlík et al. 2008), one can see a significant improvement. A main difference arises from the fact that in the previous case we generated input surface gravity disturbances from EGM96. It results in striking negative residuals in zones of the high deflections of vertical (Čunderlík et al. 2008, Fig.4) and in the overall negative bias -35 cm of the numerical solution with respect to EGM96 (Čunderlík et al. 2008, Tab.3). In this paper, input gravity data are generated from more complex and realistic sources, i.e. at first from EGM2008 and then from the DNSC08 altimetry-derived gravity data at oceans. Therefore the numerical results presented in this paper are significantly better although the numerical approach is practically the same.

In a comparison with results published in (Čunderlík and Mikula, 2009), the resolution of the new gravity field model is two times higher (0.1 deg with respect to 0.2 deg) and the iterative procedure of the elimination of far zones' interactions is introduced to reduce the initial LWES in the numerical solution. The refinement of the discretization makes the numerical solution more detailed. This can be seen from a smoother behavior of the geopotential evaluated on the DNSC08 mean sea surface comparing (Fig.8-9) with (Fig.2-3) in (Čunderlík and Mikula, 2009).

Finally we would like to outline several advantages of the presented numerical approach that could be useful for future investigations of the gravity field modelling. A main advantage consists in straightforward refining of the discretization. Although it rapidly increases memory requirements, the elimination of far zones' interactions can efficiently overcome this problem. Then it is possible to increase a resolution of the global gravity field models beyond the resolution of EGM2008. A discretization of the real Earth's surface makes the problem closer to reality. In addition, a triangulation of the Earth's surface can be done directly from points of discrete terrestrial gravimetric measurements. Therefore all drawbacks connected with an interpolation of gravity data through an evaluation of the topographic corrections can vanish. Moreover, a combination of terrestrial gravimetry with precise 3D positioning by GNSS yields consistent surface gravity disturbances those are independent from regional vertical datums. An access of such data is highly required in order to achieve

more precise global gravity field models that could be useful for solving the vertical datum problem.

7 Summary and conclusions

The direct formulation of the boundary element method gives a numerical solution to the fixed gravimetric boundary-value problem directly at points on the Earth's surface. A refinement of the discretization is essential for increasing a precision of the obtained numerical solutions. Consequently large memory requirements need to be reduced. An elimination of far zones' interactions using approximate values from satellite geopotential models is presented as an efficient tool. Inaccuracy of such approximate values leads to a long-wavelength error surface included in the obtained numerical solution that is reduced by an iterative procedure. Presented numerical experiments demonstrate how the iterative procedure tends to certain values. Such process is influenced by the distance criterion for far zones, a level of the discretization as well as accuracy of the approximate values used in the first iterative step.

The final high-resolution numerical solutions obtained by the direct BEM represent the gravity field models with the resolution 0.1 deg that is similar to the resolution of the EGM2008 geopotential model. For the test setup generated from EGM2008 the agreement with this model is better. Here the standard deviation of residuals at collocation points at oceans is 0.055 GPU (~5.6 cm). In case of the DNSC08 altimetry-derived gravity data used at oceans, the standard deviation is 0.077 GPU (~7.8 cm). It is due to negative residuals in area of the global minimum and positive residuals in area of the global maximum ranging up to ±0.3 GPU. The highest residuals are in Himalayas and Andes. They indicate a discrepancy of both gravity field models in extremely mountainous regions.

The obtained numerical results and a possibility of straightforward refinements of the discretization demonstrate the proposed approach suitable for the high-resolution global gravity field modelling. Further improvements can be achieved by a consideration of the tangential components of the oblique derivatives. Local refinements of the global solutions based on the adaptive refinement procedures are also challenging for further investigations.

References

Andersen OB, Knudsen P, Berry P (2008) The DNSC08 ocean wide altimetry derived gravity field. Presented at EGU-2008, Vienna, Austria, April, 2008

Aoyama Y, Nakano J (1999) RS/6000 SP: Practical MPI Programming. IBM, Poughkeepsie, New York

Backus GE (1968) Application of a non-linear boundary-value problem for Laplace's equation to gravity and geomagnetic intensity surveys. Q J Mech Appl Math 2: 195-221

Baláš J, Sládek J, Sládek V (1989) Stress Analysis by Boundary Element Methods. Elsevier, Amsterdam

Barrett R, Berry M, Chan TF, Demmel J, Donato J, Dongarra J, Eijkhout V, Pozo R, Romine C, Van der Vorst H (1994) Templates for the Solution of Linear Systems: Building Blocks for Iterative Methods.

http://www.netlib.org/linalg/html_templates/Templates.html

Barthelmes F, Ballani L, Klees R (1994) On the application of wavelets in geodesy. In: Geodetic Theory Today – Third Hotine–Marussi Symposium on Mathematical Geodesy, Symposium no. 114, Convened and ed. by Sanso` F. Springer, Berlin Heidelberg New York, pp 394–403

Becker JJ, Sandwell DT, Smith WHF, Braud J, Binder B, Depner J, Fabre D, Factor J, Ingalls S, Kim S-H, Ladner R, Marks K, Nelson S, Pharaoh A, Sharman G, Trimmer R, vonRosenburg J, Wallace G, Weatherall P (2009) Global Bathymetry and Elevation Data at 30 Arc Seconds Resolution: SRTM30_PLUS, revised for Marine Geodesy

Bjerhammar A, Svensson L (1983) On the geodetic boundary-value problem for a fixed boundary surface - satellite approach. Bull. Géod., 57: 382-393

Brebbia CA, Telles JCF, Wrobel LC (1984) Boundary Element Techniques, Theory and Applications in Engineering. Springer-Verlag, New York.

Čunderlík R, Mikula K (2009) On high-resolution global gravity field modelling by direct BEM using DNSC08. In: Gravity, Geoid and Earth Observation, IAG Symposia, Vol. 134, Springer (accepted in december 2008, in press)

Čunderlík R, Mikula K, Mojzeš M (2002) 3D BEM application to Neumann geodetic BVP using the collocation with linear basis functions. In: Proceedings of contributed papers and posters, ALGORITMY 2002, Conference on Scientific Computing, Vysoké Tatry-Podbanské, pp 268-275.

Čunderlík R, Mikula K, Mojzeš M (2008) Numerical solution of the linearized fixed gravimetric boundary-value problem. J Geod 82: 15-29

Fašková Z (2008) Numerical Methods for Solving Geodetic Boundary Value Problems, PhD Thesis, Svf STU Bratislava, Slovakia

Fašková Z, Čunderlík R, Janák J, Mikula K, Šprlák M (2007) Gravimetric quasigeoid in Slovakia by the finite element method, Kybernetika, Vol. 43, No. 6, pp. 789-796

Grafarend EW (1989) The geoid and the gravimetric boundary-value problem. Rep 18 Dept Geod, The Royal Institute of Technology, Stockholm

Greengard L, Rokhlin V (1987) A fast algorithm for particle simulation. J Comp. Physics, 73, 325-348.

Hackbusch W, Nowak ZP (1989) On the fast matrix multiplication in the boundary element method by panel clustering. Numerische Mathmatik, 54: 463-491

Klees R (1992) Loesung des fixen geodaetischen Randwertproblems mit Hilfe der Randelementmethode. DGK, Reihe C, Nr. 382, Muenchen

Klees R (1998) Topics on Boundary Element Methods. In: Sanso F, Rummel R (Eds.), geodetic boundary value problems in view of the one centimeter geoid. Lecture Notes in Earth Sciences Vol 65, Springer: 482-531

Klees R, Van Gelderen M, Lage C, Schwab C (2001) Fast numerical solution of the linearized Molodensky problem. J. Geod, 75: 349-362

Koch KR, Pope AJ (1972) Uniqueness and existence for the geodetic boundary value problem using the known surface of the earth, Bull. Géod., 46: 467-476

Lehmann R (1997) Studies on the Use of Boundary Element Methods in Physical Geodesy. Publ. German Geodetic Commission, Series A, No. 113. Munich

Lehmann R, Klees R (1996) Parallel Setup of Galerkin Equation System for a Geodetic Boundary Value Problem. In: Hackbusch W, Wittum G (Eds.): "Boundary Elements: Implementation and Analysis of Advanced Algorithms", Notes on Numerical Fluid Mechanics Vol. 54. Vieweg Verlag, Braunschweig

Lemoine FG, Kenyon SC, Factor JK, Trimmer RG, Pavlis NK, Chinn DS, Cox CM, Klosko SM, Luthcke SB, Torrence MH, Wang YM, Williamson RG, Pavlis EC, Rapp RH,

Olson TR (1998) EGM-96 - The Development of the NASA GSFC and NIMA Joint Geopotential Model. NASA Technical Report TP-1998-206861

Mallat SG (1989) A theory for multiresolution signal decomposition: the wavelet representation. IEEE Trans Patt Anal Mach Intell II 7: 674–693

Mayer-Gürr, T. (2007) ITG-Grace03s: The latest GRACE gravity field solution computed in Bonn, presentation at GSTM+SPP, 15-17 Oct 2007, Potsdam

Pavlis NK, Holmes SA, Kenyon SC, Factor JK (2008) An Earth Gravitational Model to Degree 2160: EGM2008, presented at the 2008 General Assembly of EGU, Vienna, Austria, April 13-18, 2008

Sacerdote F, Sansó F (1989) On the analysis of the fixed-boundary gravimetric boundary-value problem. In: Sacerdote F, Sansó F (eds) Proc 2nd Hotine-Marussi Symp Math Geod, Pisa, 1989, Politecnico di Milano, pp 507-516

Schatz AH, Thomée V, Wendland WL (1990) Mathematical Theory of Finite and Boundary Element Methods. Birkhäuser Verlag, Basel · Boston · Berlin

N	Mesh size h	Bias $[km^2.s^{-2}]$	$\|\| T - T^{ex} \|\|_{L2}$ $[km^2.s^{-2}]$	EOC
5 402	3°	-0.06828	0.002469	-
12 152	2°	-0.03033	0.001085	2.028
21 602	1.5°	-0.01705	0.000604	2.036
48 602	1°	-0.00757	0.000263	2.051
60 002	0.9°	-0.00613	0.000212	2.046
86 402	0.75°	-0.00426	0.000145	2.083
124 418	0.625°	-0.00296	0.000099	2.093
177 506	0.523°	-0.00207	0.000068	2.108

Tab.1: The experimental order of convergence (EOC) of the numerical method by the direct BEM in case of the gravitational potential generated by the artificial sphere

Number of points: N		48 602	60 002	86 402	124 418	177 506	375 002	1 215 002	4 860 002
Resolution: $\Delta\varphi$		1°	0.9°	0.75°	0.625°	0.523°	0.36°	0.2°	0.1°
Far zones' dist. criterion		no	no	no	no	no	3 189 km	911 km	213 km
Memory require-ments	Dense M	18 GB	27 GB	56 GB	116 GB	235 GB	1.05 TB	10.75 TB	171.9 TB
	Sparse M	18 GB	27 GB	56 GB	116 GB	235 GB	110.2 GB	82.49 GB	79.19 GB
% of full matrix		100%	100%	100%	100%	100%	10.2%	0.75%	0.05%

Tab.2: Levels of the disctretization and the corresponding memory requirements for the dense system matrix and for the sparse one obtained by the elimination of far zones' interactions

Setup	EGM2008				DNSC08			
Iteration	Mean	St.Dev.	Max.	Min.	Mean	St.Dev.	Max.	Min.
1	-0.0226	0.0661	0.2248	-0.6194	-0.0075	0.0876	0.2901	-0.6399
2	0.0001	0.0519	0.2178	-0.6049	0.0044	0.0758	0.2906	-0.6210
3	-0.0197	0.0552	0.2123	-0.6178	-0.0068	0.0777	0.2805	-0.6335
4	-0.0039	0.0548	0.2175	-0.6082	0.0039	0.0774	0.2911	-0.6227
5	-0.0102	0.0547	0.2142	-0.6137	-0.0013	0.0774	0.2859	-0.6279
6	-0.0103	0.0547	0.2141	-0.6136	-0.0014	0.0774	0.2858	-0.6280

Tab.3: Statistical characteristics of residuals between the numerical solution by BEM of the resolution 0.1 deg (4 860 002 collocation points) and EGM2008 at oceans using the iterative procedure of the elimination of far zones' interactions.
All values are in GPU (1 GPU = 10 $m^2.s^{-2}$).

Number of points: N		124 418	177 506	375 002	1 215 002	4 860 002
Resolution: $\Delta\varphi$		0.625°	0.523°	0.36°	0.2°	0.1°
System matrix		dense	dense	Sparse	sparse	sparse
Far zones' dist. criterion		-	-	3 189 km	911 km	213 km
Residuals at oceans (BEM - EGM2008) [GPU]	Mean	0.279	-0.294	-0.119	-0.035	-0.010
	St.Dev.	0.642	0.572	0.255	0.081	0.055
	Max.	6.663	4.375	3.290	1.016	0.214
	Min.	-4.624	-4.521	-2.845	-0.916	-0.614
Residuals on lands (BEM - EGM2008) [GPU]	Mean	0.218	-0.222	-0.255	-0.049	-0.003
	St.Dev.	1.153	0.798	0.527	0.192	0.140
	Max.	15.870	9.641	7.640	4.112	3.819
	Min.	-10.298	-7.819	-8.082	-3.401	-1.402
Total memory requirements		116 GB	235 GB	121 GB	102 GB	119 GB
Number of processors		16	16	16	16	16
CPU time / processor [h:m:s]	matrix assembly	0:11:03	0:30:16	0:48:31	4:24:39	103:45:58
	BiCGSTAB (iter)	0:07:58 (13)	0:11:22 (13)	0:01:47 (10)	0:02:41 (11)	0:02:50 (14)
	Total	0:19:02	0:41:60	0:50:21	4:28:12	103:49:01

Tab.4: Statistical characteristics of residuals between the numerical solution by BEM and EGM2008 for different discretization levels and computational aspects (1 GPU = 10 m^2.s^{-2})
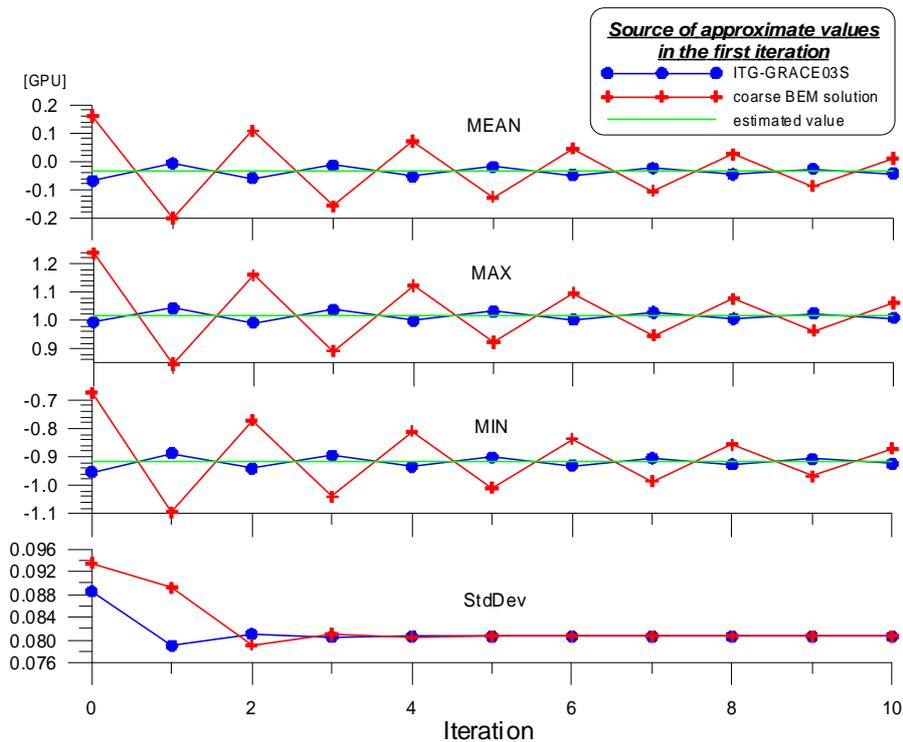
Fig.1: Statistical characteristics of residuals between the numerical solution by BEM (the resolution 0.2 deg) and EGM2008 at oceans using the iterative procedure for the elimination of far zones' interactions. Approximate values in the first iterative step are obtained (i) from the numerical solution by BEM on a coarser grid (red line), and (ii) from the ITG-GRACE03S satellite geopotential model (blue line) (1 GPU = 10 m^2.s^{-2}).
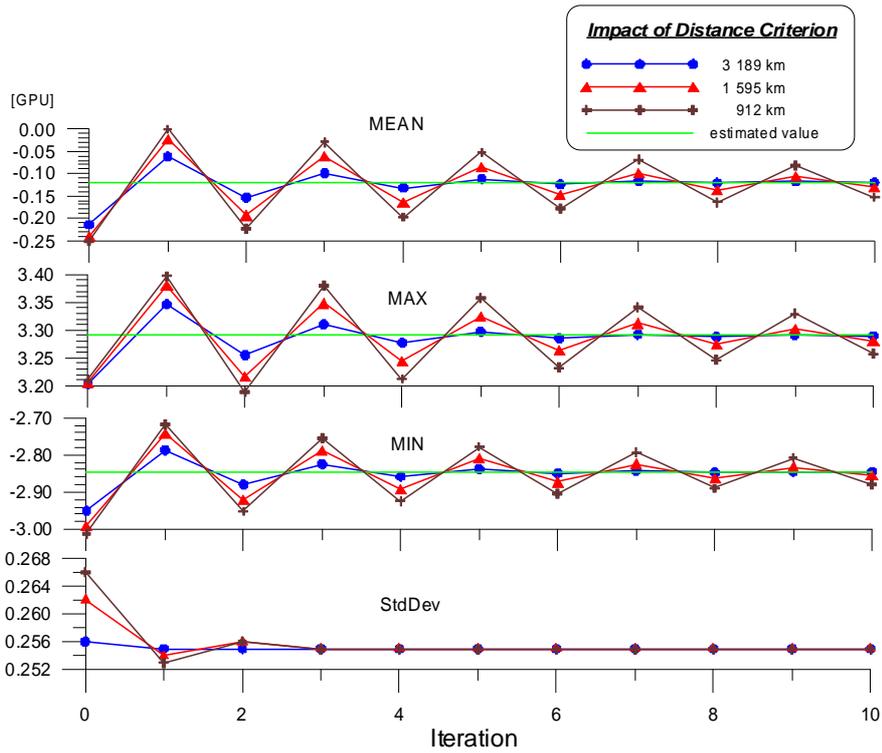
Fig.2: Statistical characteristics of residuals between the numerical solution by BEM
(the resolution 0.36 deg) and EGM2008 at oceans. The iterative procedure for the elimination
of far zones' interactions using different distance criteria:
a) blue line – 3 189 km, b) red line – 1 595 km, c) brown line – 912 km
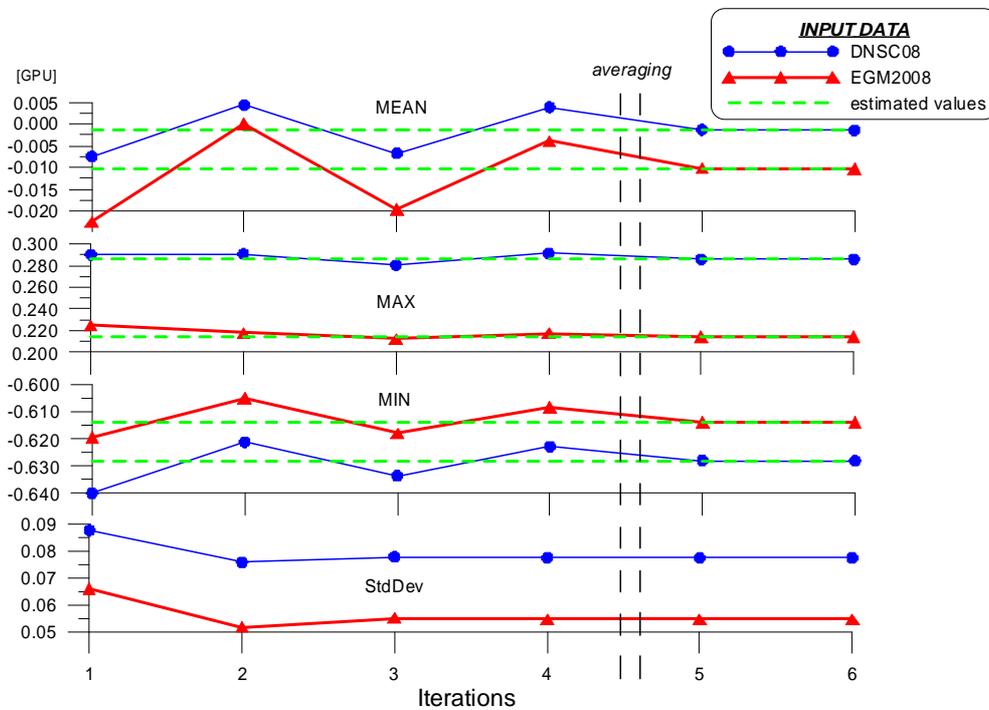
Fig.3: Statistical characteristics of residuals between the numerical solutions by BEM
(the resolution 0.1 deg) and EGM2008 at oceans. The input data are generated from (i)
EGM2008 (red line), and (ii) DNSC08 altimetry-derived gravity data (blue line).
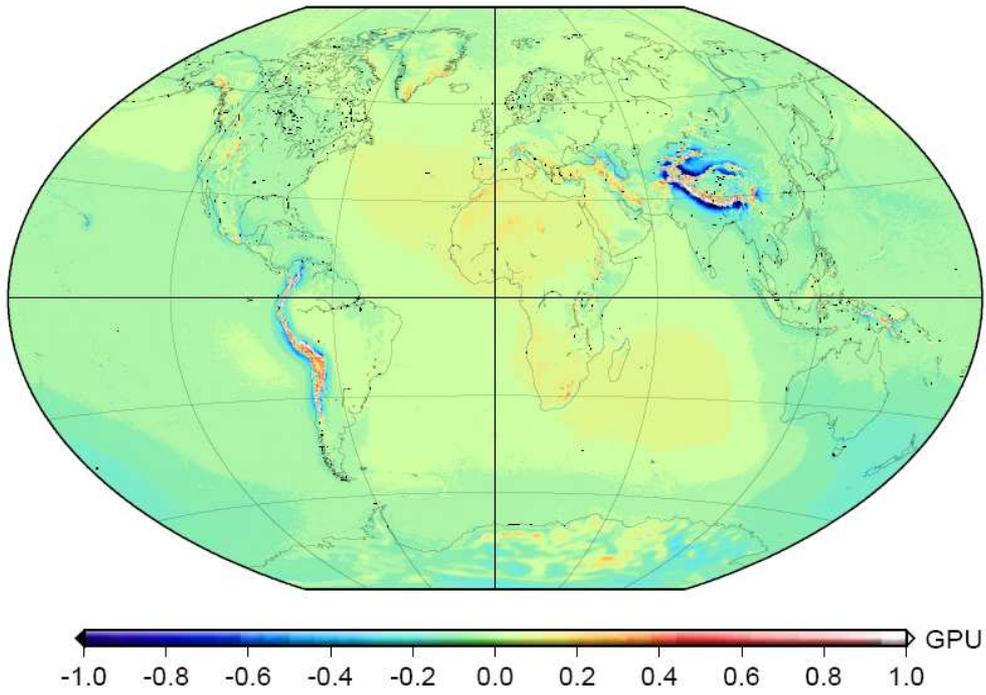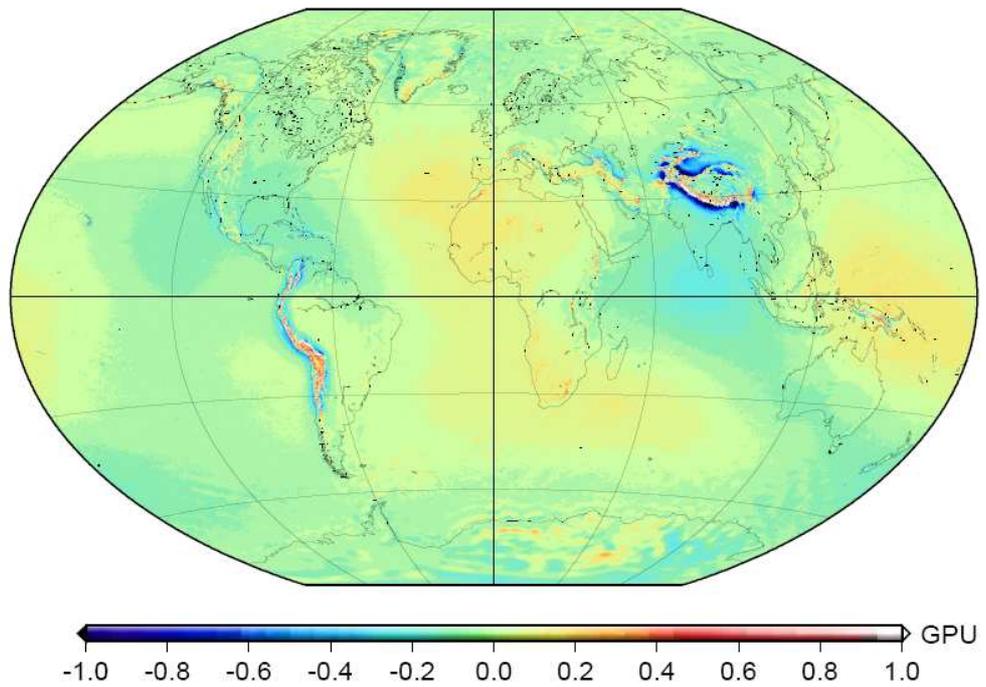
Fig.4: Residuals between the numerical solution by BEM (the resolution 0.1 deg) and EGM2008. Input data generated from a) purely EGM2008, b) DNSC08 at oceans and EGM2008 on lands
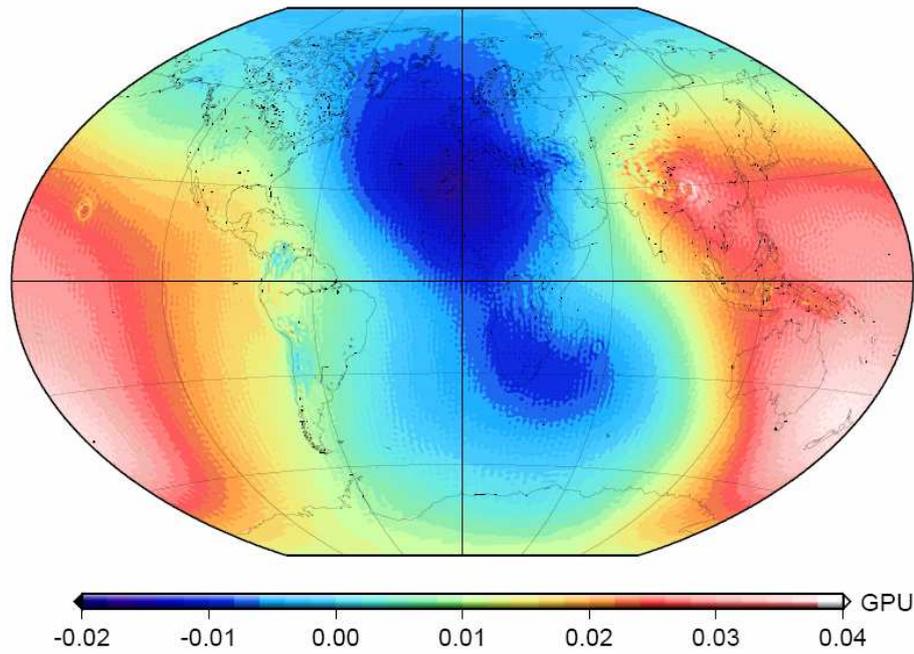
Fig.5: The long-wavelength error surface (LWES) as a difference between the numerical solutions in the last and the first iterative steps (the resolution 0.1 deg, setup from EGM2008)
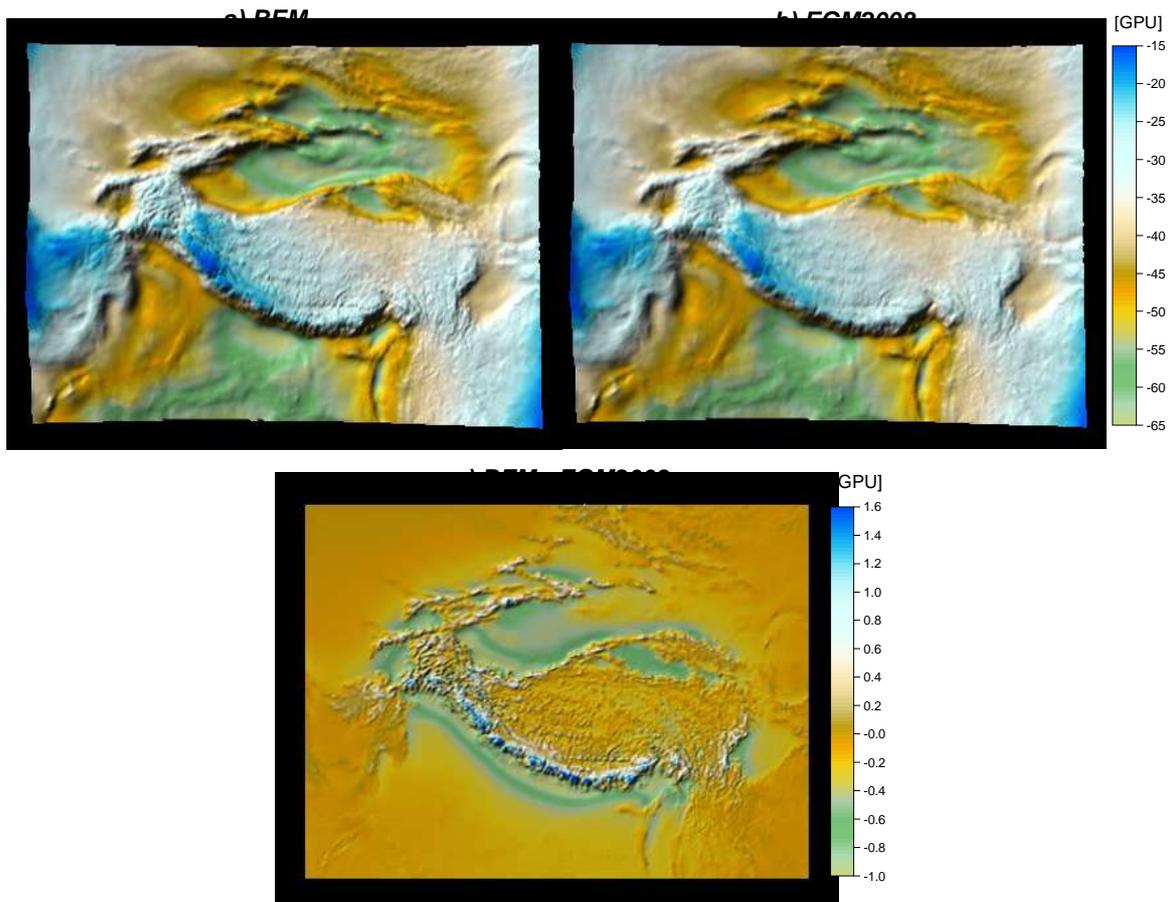
Fig.6: Details in Himalayas: a) the numerical solution by BEM (the resolution 0.1 deg), b) EGM2008, and c) residuals between both solutions
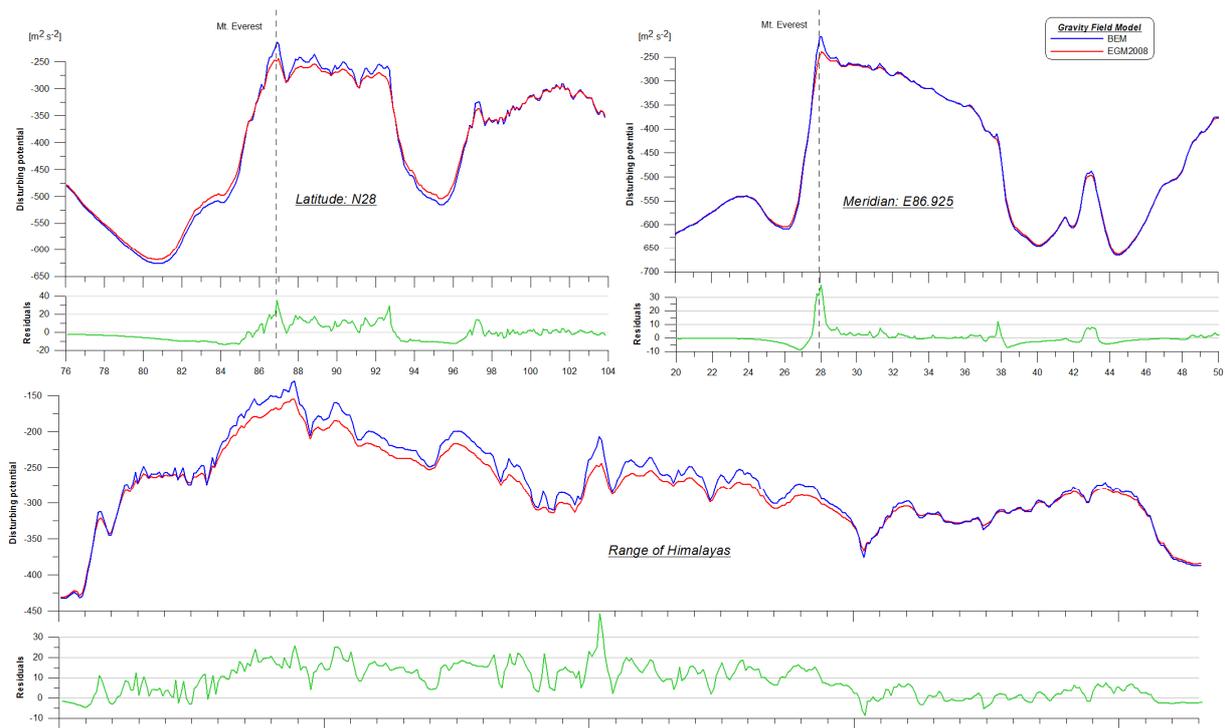
Fig.7: Profiles in Himalayas: a) the parallel of latitude crossing Mt.Everest,
b) the meridian crossing Mt.Everest, c) the main range of Himalayas (blue line - the
numerical solution by BEM, red line - EGM2008, green line – residuals BEM-EGM2008)

a) BEM   **b) EGM2008**
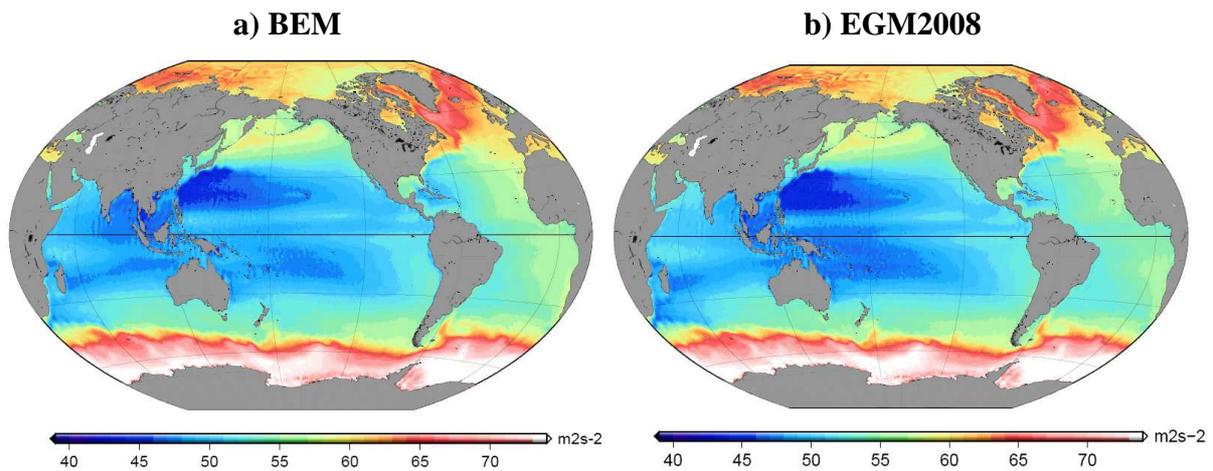
Fig.8: The geopotential on the DNSC08 mean sea surface obtained a) from the numerical
solution by BEM (the resolution 0.1 deg) and b) from EGM2008
(the constant 62 636 800.0 $m^2.s^{-2}$ is removed)

a) BEM
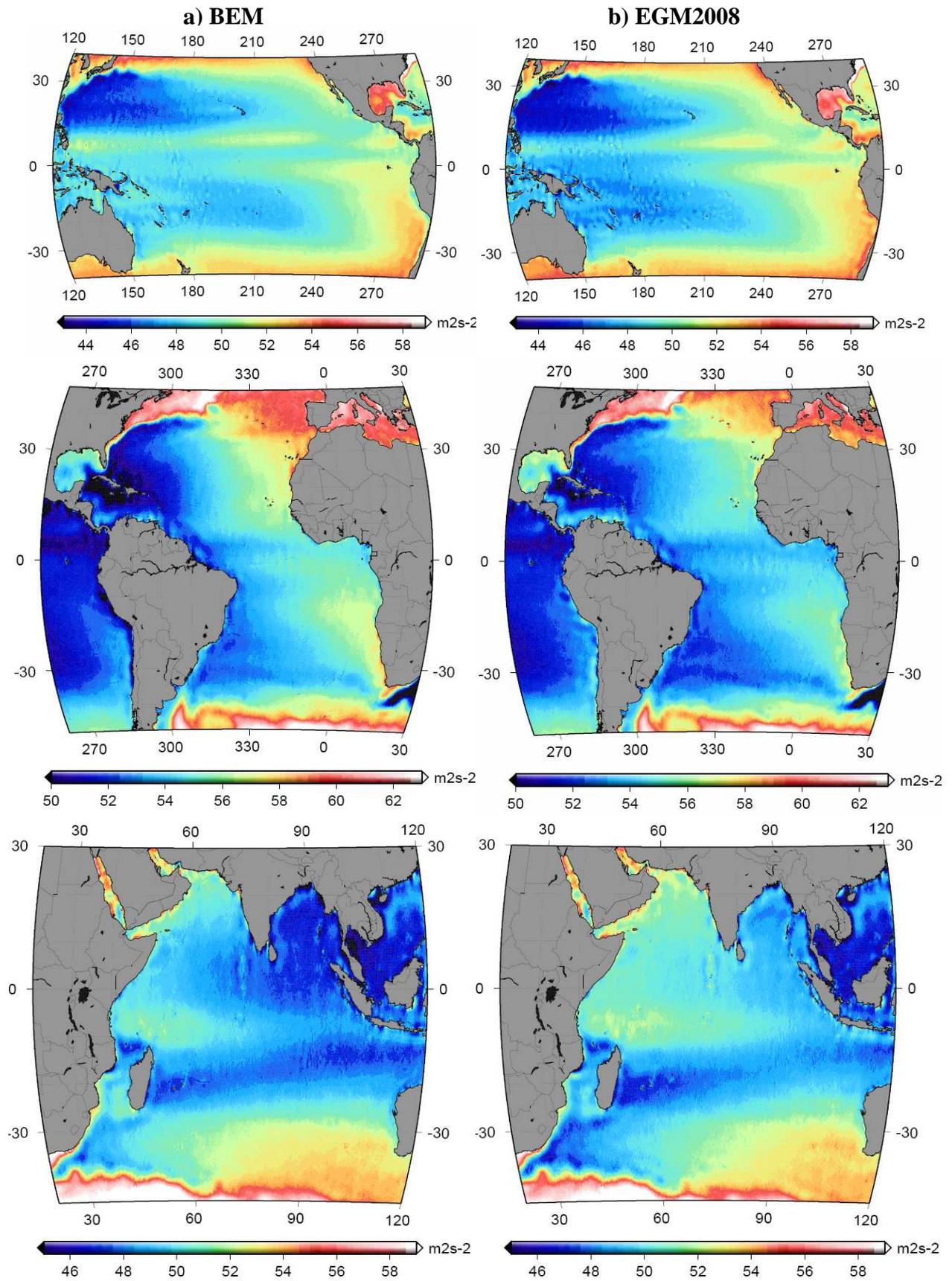
b) EGM2008

Fig.9: The geopotential on the DNSC08 mean sea surface obtained a) from the numerical solution by BEM and b) from EGM2008, details at different oceans (the constant 62 636 800.0 m^2.s^{-2} is removed)